Available online at www.sciencedirect.com

ScienceDirect

Nuclear Physics B 909 (2016) 14–42

NUCLEAR PHYSICS B

www.elsevier.com/locate/nuclphysb

Chiral random matrix model at finite chemical potential: Characteristic determinant and edge universality

Yizhuang Liu [a], Maciej A. Nowak [b], Ismail Zahed [a,*]

[a] *Department of Physics and Astronomy, Stony Brook University, Stony Brook, NY 11794-3800, USA*
[b] *M. Smoluchowski Institute of Physics and Mark Kac Complex Systems Research Center, Jagiellonian University, PL-30348 Krakow, Poland*

Received 4 February 2016; received in revised form 25 April 2016; accepted 26 April 2016

Available online 29 April 2016

Editor: Hubert Saleur

Abstract

We derive an exact formula for the stochastic evolution of the characteristic determinant of a class of deformed Wishart matrices following from a chiral random matrix model of QCD at finite chemical potential. In the WKB approximation, the characteristic determinant describes a sharp droplet of eigenvalues that deforms and expands at large stochastic times. Beyond the WKB limit, the edges of the droplet are fuzzy and described by universal edge functions. At the chiral point, the characteristic determinant in the microscopic limit is universal. Remarkably, the physical chiral condensate at finite chemical potential may be extracted from current and quenched lattice Dirac spectra using the universal edge scaling laws, without having to solve the QCD sign problem.
© 2016 The Authors. Published by Elsevier B.V. This is an open access article under the CC BY license (http://creativecommons.org/licenses/by/4.0/). Funded by SCOAP[3].

1. Introduction

QCD breaks spontaneously chiral symmetry with a wealth of evidence in hadronic processes at low energies [1]. First principle lattice simulations strongly support that [2]. The spontaneous

* Corresponding author.
E-mail addresses: yizhuang.liu@stonybrook.edu (Y. Liu), maciej.a.nowak@uj.edu.pl (M.A. Nowak), ismail.zahed@stonybrook.edu (I. Zahed).

http://dx.doi.org/10.1016/j.nuclphysb.2016.04.040
0550-3213/© 2016 The Authors. Published by Elsevier B.V. This is an open access article under the CC BY license (http://creativecommons.org/licenses/by/4.0/). Funded by SCOAP[3].

breaking is characterized by a large accumulation of eigenvalues of the Dirac operator near zero-virtuality [3]. The zero virtuality regime is ergodic, and its neighborhood is diffusive [4].

The ergodic regime of the QCD Dirac spectrum is amenable to a chiral random matrix model [5]. In short, the model simplifies the Dirac spectrum to its zero-mode-zone (ZMZ). The Dirac matrix is composed of hopping between N-zero modes and N-anti-zero modes because of chirality, which are Gaussian sampled by the maximum entropy principle. The model was initially suggested as a null dynamical limit of the random instanton model [6]. It also follows from the ϵ-expansion in QCD [7].

QCD at finite chemical potential μ is subtle on the lattice due to the sign problem [8]. A number of effective models have been proposed to describe the effects of matter in QCD with light quarks [1]. Chiral random matrix models offer a simple construct that retains some essentials of chiral symmetry both in vacuum and matter. For instance, in the chiral 1-matrix model finite μ is captured by a constant deformation of Gaussian matrix ensembles [9,10]. In the chiral 2-matrix model the deformation with μ is also random [11,12]. Chiral matrix models in matter were discussed by many [13,14]. Recently both a universal shock analysis [15] and a hydrodynamical description of the Dirac spectra were suggested [16] both at zero and finite chemical potential.

The matrix models were shown to exhibit the same microscopic universality for small eigenvalues in the ergodic regime with vanishingly small μ^2 in the large volume limit [14]. The chief observation is that in the weakly non-hermitean limit, the matrix models can be deformed in a way that preserves the global aspects of the coset manifold under the general strictures of spontaneously broken chiral symmetry and power counting in the so-called epsilon-regime [17].

At finite μ the distribution of Dirac eigenvalues in the complex plane maps onto a 2-dimensional Coulomb gas whose effective action is mostly controlled by Coulomb's law, the conformal and gravitational anomalies in 2-dimensions [16]. These constraints on the Dirac spectrum are beyond the range of chiral symmetry. The eigenvalues form Coulomb droplets that stretch and break at finite μ. The accumulation of the complex eigenvalues at the edge of the droplet may signal a new form of universality unknown to chiral symmetry. The purpose of this paper is to explore this possibility using the concept of characteristic determinants for a unitary random matrix model at finite μ.

With this in mind, we start by developing a stochastic evolution for a Wishart characteristic determinant associated to the standard chiral random matrix model for QCD Dirac spectra at finite chemical potential μ, much along the lines suggested in [15] for the Ginibre ensemble. At finite μ the eigenvalues of the Dirac operator spread in the complex plane. Their accumulation in droplets break spontaneously holomorphic symmetry [9,10]. The characteristic determinant acts as an order parameter for this breaking being zero within the droplet and finite outside. The evolution involves the eigenvalues as complex masses and their conjugates and is diffusion-like asymptotically. The universal behavior of the characteristic determinant at the edge of the Ginibre droplet observed in [15] will be exploited here to derive a universal edge behavior for the Dirac spectra at finite chemical potential.

Finally, we note that the study of deformed and non-hermitean Wishart matrices is interesting on its own as it is of interest to many other areas such as telecommunications and finances, where issues of signal to noise in the presence of attenuation or losses are relevant in designing more efficient routers or financial instruments [18].

The main and new results of the paper are the following: 1) The derivation of a closed evolution equation for the characteristic determinant for a non-hermitean deformation of Wishart matrices in relation to a 1-matrix model for the phase quenched QCD with $N_f = 2$ flavors at finite μ; 2) An explicit derivation of the envelope of the complex eigenvalues for the deformed

Wishart matrices; 3) An explicit microscopic scaling law for the distribution of the deformed Wishart eigenvalues at the edge as traced by the envelope; 4) An explicit scaling law on the real edge of the complex eigenvalue distribution that scales with the chiral condensate at finite μ, allowing its extraction from current and quenched Dirac spectra; 5) An explicit microscopic scaling law for the characteristic determinant at the chiral point that scales with infinitesimal μ.

The organization of the paper is as follows: In section 2, we review the matrix model description of the partition function for N_f flavors at finite μ and its phase quenched approximation. In section 3 we show that a pertinent characteristic determinant is the phased quenched matrix-model partition function for given N_f. We follow the recent work analysis in [15] and identify a mathematical time with a continuous deformation of the harmonic trap. We explicit the evolution equation for the characteristic determinant for $N_f = 2$ and show that it is parabolic asymptotically. In principle our method applies to any even $N_f = 2k$. However, it is much more involved analytically for $k > 1$. In section 4 we use the WKB method to solve the evolution equation for the boundary of the eigenvalue droplet in leading order. In section 5 we derive an exact solution for the evolution of the characteristic determinant using the method of characteristics. In section 6 we develop a semi-classical expansion of the exact solution to explicit the universal character of the edges of the droplet of complex Dirac eigenvalues. At the chiral point, the characteristic determinant in the microscopic limit follows from a universal Bessel kernel. Our conclusions are in section 7. In Appendix A we detail an alternative scaling law for the characteristic determinant on the real edge of the complex spectrum. In Appendix B, we briefly quote the results for the characteristic determinant following from a 2-matrix model and confirm its microscopic universality at the chiral point.

2. Chiral matrix model

The low lying eigenmodes of the QCD Dirac operator capture some aspects of the spontaneous breaking of chiral symmetry both in vacuum and in matter. Remarkably, their fluctuations follow by approximating the entries in the Dirac operator by purely random matrix elements which are chiral (paired spectrum) and fixed by time-reversal symmetry (Dyson ensembles). At finite μ the Dirac spectrum on the lattice is complex [19,20]. The matrix models at finite μ [9,11] capture this aspect of the lattice spectra and the nature of the chiral phase transition [1,13,14].

In this section, we will briefly review the salient features of the standard or 1-matrix model and explicit the relationship between the chiral Dirac ensemble and a deformed Wishart ensemble both at finite μ. For that, consider the 1-matrix model at finite chemical potential for N_f fundamental quarks in the complex representation or $\beta = 2$ [9,10]

$$\begin{aligned}\mathbf{Z}_{N_f}[\tau, \mathbf{z} = -im_f, \mu] &= \left\langle \det(\mathbf{z} - \mathbf{D})^{N_f} \right\rangle \\ &\equiv \int d\mathbf{T}\, d\mathbf{T}^\dagger\, \mathbf{P}(\tau, \mathbf{T})\, \det \begin{pmatrix} \mathbf{z} & \mathbf{T} - i\mu \\ \mathbf{T}^\dagger - i\mu & \mathbf{z} \end{pmatrix}^{N_f} \end{aligned} \tag{1}$$

for equal quark masses m_f in the complex representation. Here

$$\mathbf{P}(\tau, \mathbf{T}) = e^{-\frac{N}{\tau}\mathrm{Tr}(\mathbf{T}^\dagger \mathbf{T})} \tag{2}$$

and $\mathbf{T}$ is $(N + \nu) \times N$ valued complex matrix. ν accounts for the difference between the number of zero modes and anti-zero modes. The chiral Dirac matrix $\mathbf{D}$ in (1) has ν unpaired zero modes and N paired eigenvalues $\pm i z_j$ in the massless limit. The paired eigenvalues delocalize and are represented by (1). The unpaired zero-modes decouple. Throughout we will set $\nu = 0$ and $\mathbf{T}$ is

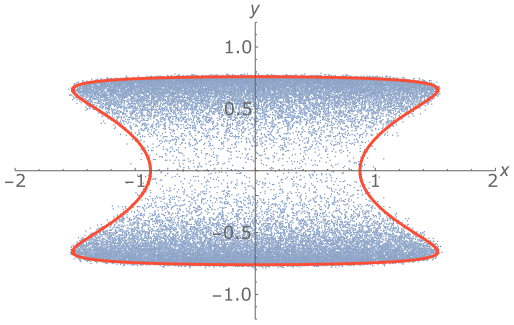

Fig. 1. Eigenvalue distribution for the chiral Dirac matrices **D** for $\mu/\mu_c = 0.9$ and $\tau = 1$.

a square complex matrix. In the vacuum, the Banks–Casher formula [3] fixes the dimensionful parameter to a constant $\tau \to 1/a$ with $\sqrt{a} = |q^\dagger q|_0/\mathbf{n}$ in terms of the massless quark condensate and the density of zero modes $\mathbf{n} = N/V_4$.

In Fig. 1 we display the distribution of eigenvalues following from the 1-matrix model with **T** sampled from a Gaussian ensemble of 200×200 matrices with $\nu = 0$ and $\mu = 0.9$. The eigenvalue distribution forms a connected droplet in the z-plane for $\mu < \mu_c = \sqrt{\tau}$, and splits into two droplets symmetric about the real-axis for $\mu > \mu_c = \sqrt{\tau}$, restoring chiral symmetry [9,10]. In the spontaneously broken phase, all droplets are connected and symmetric about the real-axis. Some of these feature are shared by the lattice droplets of Dirac eigenvalues [19,20].

The complex nature of the eigenvalues entering in the determinant in (1) yields to the so-called sign problem when evaluating the complex partition function. A simplifying assumption known as the quenched approximation used in earlier lattice simulations, consists in dropping the phase of the determinant. In the 1-matrix model this amounts to using

$$\mathbb{Z}_{N_f}[\tau, \mathbf{z} = -im_f, \mu] = \left\langle \det |\mathbf{z} - \mathbf{D}|^{N_f} \right\rangle \tag{3}$$

where the averaging is carried using (2). This approximation yields to subtleties as discussed in [9]. While the phase factor is subleading in $1/N$ at the macroscopic level [21], its effects at the microscopic limit are not [22]. If we set $z = \mathbf{z}^2 + \mu^2$, (3) can be re-written as

$$\mathbb{Z}_{N_f}[\tau, z, \mu] = \left\langle |\det (z - \mathbf{W})|^{N_f} \right\rangle \tag{4}$$

with the deformed Wishart matrix

$$\mathbf{W} = \mathbf{T}^\dagger \mathbf{T} - i\mu(\mathbf{T}^\dagger + \mathbf{T}) \tag{5}$$

The eigenvalue distribution for the deformed Wishart matrices (5) is shown in Fig. 2 for 20×20 matrices sampled from a similar Gaussian ensemble with $\mu/\mu_c = 0.9$. The droplet spreads and stretches vertically for increasing μ but does not break. The density of eigenvalues within the droplets in Figs. 1, 2 breaks spontaneously conformal symmetry [9,10]. This breaking is best captured through the following regulated partition function

$$Z_{N_f}[\tau, z, w, \mu] \equiv \left\langle \left(\det \left(|z - \mathbf{W}|^2 + \overline{w} w \right) \right)^{\frac{N_f}{2}} \right\rangle \tag{6}$$

which gives the partition function in the double limit

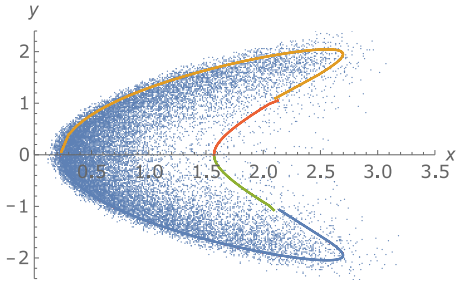

Fig. 2. Eigenvalue distribution for the deformed Wishart **W** matrices for $\mu/\mu_c = 0.9$ and $\tau = 1$.

$$\mathbb{Z}_{N_f}[\tau, z, \mu] = \lim_{w\to 0}\lim_{N\to\infty} Z_{N_f}[\tau, z, w, \mu] \tag{7}$$

The measure in (1)–(6) acts as a harmonic trap for the complex eigenvalues that are deformed and split by the chemical potential. Following [15] we will identify τ with a mathematical and continuous time deformation of the harmonic trap. Eq. (2) satisfies the formal matrix diffusion equation

$$N\partial_\tau \mathbf{P} = \frac{\partial^2 \mathbf{P}}{\partial \mathbf{T}^\dagger \partial \mathbf{T}} \qquad \text{with} \qquad \mathbf{P}(0, \mathbf{T}) \approx \delta(\mathbf{T}) \tag{8}$$

Eq. (8) shows that the diffusive equation is purely kinetic with no potential or pressure like contribution. This is to be contrasted with the many-body hydrodynamics expansion of the Dirac eigenvalues where both kinetic and pressure terms are identified in the Eulerian flow in [16].

3. Diffusion

In this section we will define a pertinent characteristic determinant that will be used to analyze the nature and evolution of the complex eigenvalues of the deformed Wishart ensemble. We will show that the evolution of the characteristic determinant obeys a non-local equation that is diffusion-like asymptotically.

Indeed, a simple understanding of the accumulation and diffusion of the eigenvalues of the Dirac operator in the complex plane follows by identifying the phase quenched and regulated partition function (6) for $N_f = 2$ with the characteristic determinant

$$\mathbf{\Psi}(\tau, z, w) \equiv Z_{N_f=2}[\tau, z, w, \mu] \tag{9}$$

Eq. (9) defines a $2N$-degree polynomial which asymptotes $|z|^{2N}$ [13]. The zeros of the characteristic determinant are the complex eigenvalues of the deformed Wishart matrix **W** in (5). They are related to the eigenvalues of the Dirac operator **D** in the complex 2-plane by recalling the mapping $z = \mathbf{z}^2 + \mu^2$. The macroscopic density of complex and deformed Wishart eigenvalues is

$$\rho_W(\tau, z) = \lim_{w\to 0}\lim_{N\to\infty} \frac{1}{N\pi}\partial^2_{z\bar{z}} \ln \mathbf{\Psi}(\tau, z, w) \tag{10}$$

with $\ln\mathbf{\Psi}/N$ acting as a Coulomb-like potential at large N. The corresponding eigenvalue density for the chiral Dirac operator as a function of τ, follows from (10) through

$$\rho_D(\tau, \mathbf{z}) = 2|\mathbf{z}|\, \rho_W(\tau, \mathbf{z}^2 + \mu^2) \tag{11}$$

The eigenvalues condense in a droplet, with $\mathbf{\Psi} \approx 0$ inside and $\mathbf{\Psi}/|z|^{2N} \approx 1$ (order parameter), as the corresponding pressure $\ln\mathbf{\Psi}$ changes sign across the droplet boundary (phase change) [10,13].

Unwinding the determinant in $\mathbf{\Psi}$ through a Grassmannian quark q and conjugate quark Q, yields

$$\begin{aligned}
&\mathbf{\Psi}(\tau, z, w) \equiv \left\langle e^{\mathbf{F}+\mathbf{G}} \right\rangle \\
&\equiv \int d\mathbf{T} d\mathbf{T}^\dagger dq\, dq^\dagger\, dQ\, dQ^\dagger\, \mathbf{P}(\tau, \mathbf{T}) \\
&\times\ e^{q^\dagger(z-\mathbf{W})q + Q^\dagger(\bar{z}-\mathbf{W}^\dagger)Q - \bar{w}q^\dagger Q + wQ^\dagger q}
\end{aligned} \tag{12}$$

where we have defined

$$\begin{aligned}
\mathbf{F} &= q^\dagger(z-\mathbf{W})q + Q^\dagger(\bar{z}-\mathbf{W}^\dagger)Q \\
\mathbf{G} &= -\bar{w}q^\dagger Q + wQ^\dagger q
\end{aligned} \tag{13}$$

Note that the complex eigenvalues z, $\bar{z}$ act as complex masses for the pair of quark bilinears $q^\dagger q$, $Q^\dagger Q$, while w, $\bar{w}$ act as complex mixing masses for the pair of mixed quark bilinears $Q^\dagger q$ and $q^\dagger Q$. The formers preserve holomorphy, while the latters do not [13]. (12) obeys the evolution equation

$$\begin{aligned}
&N\partial_\tau \mathbf{\Psi}(\tau, z, w, \mu) = \\
&\Big\langle \Big(-N(q^\dagger q + Q^\dagger Q) \\
&- q^\dagger q q^\dagger \mathbf{W} q - Q^\dagger Q Q^\dagger \mathbf{W}^\dagger Q - q^\dagger Q Q^\dagger \mathbf{W} q - Q^\dagger q q^\dagger \mathbf{W}^\dagger Q \\
&+ 2i\mu\, Q^\dagger q q^\dagger \mathbf{T} Q - 2i\mu\, q^\dagger Q Q^\dagger \mathbf{T} q \\
&- 2\mu^2 q^\dagger Q Q^\dagger q + \mu^2\ (q^\dagger q + Q^\dagger Q) \Big)\, e^{\mathbf{F}+\mathbf{G}} \Big\rangle
\end{aligned} \tag{14}$$

where we have used (8). With the help of the identity

$$\begin{aligned}
&\left\langle \left(+2i\mu\, Q^\dagger q q^\dagger \mathbf{T} Q - 2i\mu\, q^\dagger Q Q^\dagger \mathbf{T} q \right)\, e^{\mathbf{F}+\mathbf{G}} \right\rangle \\
&= -4\mu^2\tau^2 \frac{\partial_w \partial_{\bar{w}} (\partial_w \partial_{\bar{w}} + \partial_z \partial_{\bar{z}})}{(1-\tau\partial_z)(1-\tau\partial_{\bar{z}}) + \tau^2 \partial_w \partial_{\bar{w}}} \left\langle e^{\mathbf{F}+\mathbf{G}} \right\rangle
\end{aligned} \tag{15}$$

most of the terms on the right-hand-side of (14) can be turned either to ordinary z-derivatives of $e^{\mathbf{F}}$ or some Grassmannian derivative of $e^{\mathbf{F}}$ or $e^{\mathbf{G}}$. The final result is a closed but non-local evolution of the characteristic determinant (12), i.e.

$$\begin{aligned}
N\partial_\tau \mathbf{\Psi} = \Bigg(&- 2(\partial_z + \partial_{\bar{z}}) \\
&- (z\partial_z^2 + \bar{z}\partial_{\bar{z}}^2 - (z+\bar{z})\partial_{\bar{w}w}^2) \\
&- (\partial_z + \partial_{\bar{z}})(w\partial_w + \bar{w}\partial_{\bar{w}}) \\
&+ 2\mu^2 \partial_{\bar{w}w}^2 + \mu^2(\partial_z^2 + \partial_{\bar{z}}^2) \\
&- \left(\frac{2\mu\tau}{N}\right)^2 \frac{\partial_w \partial_{\bar{w}} (\partial_w \partial_{\bar{w}} + \partial_z \partial_{\bar{z}})}{\left|1 - \frac{\tau}{N}\partial_z\right|^2 + \left|\frac{\tau}{N}\partial_w\right|^2} \Bigg) \mathbf{\Psi}
\end{aligned} \tag{16}$$

which is diffusive-like or parabolic at asymptotic times, subject to the initial condition

$$\mathbf{\Psi}(\tau = 0, z, w) = (|z_0|^2 + |w_0|^2)^N \tag{17}$$

Eqs. (16)–(17) is the first main result of this paper.

The stochastic evolution of $\mathbf{\Psi}$ involves the evolution in both the normal z, $\bar{z}$ and mixed w, $\bar{w}$ masses to allow for the spontaneous breaking of chiral symmetry as well as the spontaneous breaking of holomorphy, respectively. The spontaneous breaking of chiral symmetry is signaled by the accumulation of Dirac eigenvalues around zero or $\mathbf{z} = 0$ ($z = \mu^2$), i.e. a non-vanishing $\langle q^\dagger q \rangle$. The spontaneous breaking of holomorphy is signaled by the spreading of Dirac eigenvalues in the complex plane, i.e. a non-vanishing $\langle |q^\dagger Q|^2 \rangle$ [9,10,13].

4. WKB approximation

In this section we will provide a WKB analysis of the non-local and diffusion-like equation for the characteristic determinant derived in the previous section. We will use it to derive a polynomial and parametric equation for the time-dependent envelope of the complex eigenvalues for the deformed Wishart ensemble, and by mapping for the standard but diffusing Dirac ensemble at finite μ.

Eq. (16) is a non-local Schroedinger-like evolution equation in Euclidean time. Some insights to this evolution can be obtained using the WKB method in the large $N(= 1/\hbar)$ limit. For that we identify

$$\mathbf{\Psi} \approx e^{N\mathbb{S}} \tag{18}$$

in (16) and define the conjugate momenta $p_\xi = \partial_\xi \mathbb{S}$ with $\xi = z, \bar{z}, r = \sqrt{w\bar{w}}$. Note that in leading N, the eigenvalue density for the deformed Wishart class in (5) is given by

$$\rho_W(\tau, z) = \lim_{w\to 0} \frac{1}{\pi} \partial_{\bar{z}} p_z \tag{19}$$

which is non-holomorphic inside the droplet.

4.1. Hamilton–Jacobi equations

Using the rescaling $N\tau \to \tau$, the effective semi-classical action $\mathbb{S}$ obeys

$$\partial_\tau \mathbb{S} + \mathbb{H}(\tau, \xi, p_\xi) = 0 \tag{20}$$

with the τ-dependent and non-local effective Hamiltonian

$$\begin{aligned}\mathbb{H} = &+ z p_z^2 + \bar{z} p_{\bar{z}}^2 - (z + \bar{z}) p_r^2/4 \\ &+ r(p_z + p_{\bar{z}}) p_r - \mu^2 (p_z^2 + p_{\bar{z}}^2) - \frac{\mu^2 p_r^2}{2} \\ &+ \mu^2 \tau^2 \frac{p_r^2 (\frac{p_r^2}{4} + p_z p_{\bar{z}})}{(1 - \tau p_z)(1 - \tau p_{\bar{z}}) + \tau^2 \frac{p_r^2}{4}}\end{aligned} \tag{21}$$

The initial condition is $\mathbb{S}(0) = \ln(|z_0|^2 + r_0^2)$.

The semi-classical equations are the standard Hamilton–Jacobi equations,

$$\begin{aligned}
\frac{dp_z}{d\tau} &= -\frac{\partial \mathbb{H}}{\partial z} = -p_z^2 + p_r^2/4 \\
\frac{dp_{\bar{z}}}{d\tau} &= -\frac{\partial \mathbb{H}}{\partial \bar{z}} = -p_{\bar{z}}^2 + p_r^2/4 \\
\frac{dp_r}{d\tau} &= -\frac{\partial \mathbb{H}}{\partial r} = -p_r(p_z + p_{\bar{z}})
\end{aligned} \tag{22}$$

which are readily integrated

$$\begin{aligned}
p_x(\tau) &= \frac{x_0 + \tau}{(x_0+\tau)^2 + y_0^2 + r_0^2} \\
p_y(\tau) &= \frac{-y_0}{(x_0+\tau)^2 + y_0^2 + r_0^2} \\
p_r(\tau) &= \frac{2r_0}{(x_0+\tau)^2 + y_0^2 + r_0^2}
\end{aligned} \tag{23}$$

and

$$\begin{aligned}
\frac{dz}{d\tau} &= \frac{\partial \mathbb{H}}{\partial p_z} \\
\frac{dr}{d\tau} &= \frac{\partial \mathbb{H}}{\partial p_r}
\end{aligned} \tag{24}$$

which are in general involved.

4.2. Expanding droplet boundary

The initialization of the characteristic determinant through (18) at the droplet edge or $r_0 = 0$, allows for a simplification of (24) at the edge. Indeed, (24) for $z(\tau)$ at the edge, yields

$$\frac{z(\tau) - \mu^2}{z_0 - \mu^2} = \left(1 + \frac{\tau}{z_0}\right)^2 \tag{25}$$

while (24) for small $r(\tau)$ gives

$$\begin{aligned}
\frac{dr}{d\tau} &= f_1(\tau) r + r_0 f_2(\tau) \\
f_1(\tau) &= \frac{1}{z_0 + \tau} + \frac{1}{\bar{z}_0 + \tau} \\
f_2(\tau) &= -\frac{4\mu^2\left(1 - \frac{\tau^2}{|z_0|^2}\right) + \left((z_0 - \mu^2)(1 + \frac{\tau}{z_0}) + \text{c.c.}\right)}{(x_0+\tau)^2 + y_0^2}
\end{aligned} \tag{26}$$

The formal solution of (26) is

$$r(\tau) = r_0 \left(1 + \int_0^\tau d\tau' f_2(\tau') e^{-\int_0^{\tau'} d\tau'' f_1(\tau'')}\right) e^{\int_0^\tau d\tau' f_1(\tau')} \tag{27}$$

The boundary of the eigenvalue droplet is set by the condition

$$1+\int_0^{\tau} f_2(\tau')e^{-\int_0^{\tau'} f_1(\tau'')d\tau''}d\tau'=0 \tag{28}$$

Inserting

$$e^{-\int_0^{\tau'} f_1(\tau'')d\tau''}=\frac{|z_0|^2}{(x_0+\tau')^2+y_0^2} \tag{29}$$

in (28) and using

$$\begin{aligned}&\int_0^{\tau} d\tau' \frac{x_0^2+y_0^2-\tau'^2}{|(x_0+\tau')^2+y_0^2|^2}=\frac{\tau}{(x_0+\tau)^2+y_0^2}\\ &\int_0^{\tau} d\tau' \frac{(x_0+iy_0+\tau')^2}{|(x_0+\tau')^2+y_0^2|^2}=\frac{\tau}{\bar{z}_0(\bar{z}_0+\tau)}\end{aligned} \tag{30}$$

yield the polynomial condition for $z_0=x_0+iy_0$

$$\frac{4\mu^2\tau}{(x_0+\tau)^2+y_0^2}+\frac{z_0-\mu^2}{z_0}\frac{\tau}{\bar{z}_0+\tau}+\frac{\bar{z}_0-\mu^2}{\bar{z}_0}\frac{\tau}{z_0+\tau}=1 \tag{31}$$

A simple check of the result (31) follows for $\mu=0$, for which we have

$$z_0+\bar{z}_0+2\tau=\frac{1}{\tau}(z_0+\tau)(\bar{z}_0+\tau) \tag{32}$$

The general solution is $z_0=\tau e^{i\theta}$. Inserting this solution in (25), we have

$$z(\tau)=\tau(2+e^{-i\theta}+e^{i\theta})=4\cos^2(\theta/2) \tag{33}$$

which is the support of the τ-expanding Wishart line segment on the real-axis, i.e. $[0,4\tau]$. For general μ, (31) yields the expanding 4 branches ($\mathbf{s},\mathbf{s}'=\pm$)

$$y_0^{\mathbf{s}\mathbf{s}'}(x_0)= \tag{34}$$

$$\mathbf{s}\tau\left(-\frac{x_0^2}{\tau^2}+\left(\frac{1}{2}+\frac{\mu^2}{\tau}\right)\left(1+\mathbf{s}'\left(1-\frac{8\mu^2x_0}{(\tau+2\mu^2)^2}\right)^{\frac{1}{2}}\right)\right)^{\frac{1}{2}}$$

which once inserted in (31) give a parametric description of the evolving τ-expanding boundary, as the envelope of the eigenvalues of the deformed Wishart eigenvalues as shown in Fig. 2. We have explicitly checked that the envelope for the distributions of Dirac eigenvalues in Fig. 1 follows from the deformed Wishart envelope by using the inverse mapping $\mathbf{z}=\pm\sqrt{z-\mu^2}$. It is in agreement with the original envelope obtained in [9,10] using different arguments.

5. Characteristic determinant

In this section, we will provide a formal solution for the stochastically evolving characteristic determinant for the deformed Wishart ensemble, that is exact for finite size N and time τ. For

that, we will use the method of characteristics to solve exactly the partial differential equation (16) in Fourier space.

A formal but exact solution to the diffusion-like equation (14) for the characteristic determinant can be obtained by recasting (16) in conjugate or Fourier space. Specifically,

$$\mathbf{\Psi}(\tau, z, w) = \int \frac{d^2k}{(2\pi)^2} \frac{d^2p}{(2\pi)^2} e^{ik\cdot w + ip\cdot z}\ \tilde{\mathbf{\Psi}}(\tau, k, p) \tag{35}$$

Taking the Fourier transform of (16) yields

$$N\partial_\tau \tilde{\mathbf{\Psi}} = \tilde{\mathbb{H}}\,\tilde{\mathbf{\Psi}} \tag{36}$$

with the conjugate Hamiltonian

$$\begin{aligned}\tilde{\mathbb{H}} &= 2p_1 + \frac{\mu^2}{2}(k^2 + p_1^2 - p_2^2)\\ &- \frac{\mu^2\tau^2}{4N^2}\frac{k^2(p^2+k^2)}{(1-\frac{\tau p_1}{2N})^2 + \frac{\mu^2\tau^2}{N^2}\frac{p_2^2+k^2}{4}}\\ &+ \frac{p_1^2 - p_2^2 - k^2}{2}\partial_{p_1} + p_1 p_2 \partial_{p_2} + p_1 k \partial_k\end{aligned} \tag{37}$$

after the shifts $k \to -ik$ and $p \to -ip$. Here k is the conjugate to $\sqrt{w\bar{w}} \equiv r$.

5.1. Characteristic lines

The evolution equation (36) is now first order with rational coefficients. It can be solved by the characteristic method exactly. The characteristic lines are

$$\begin{aligned}\frac{d\tau}{ds} &= N\\ \frac{dp_1}{ds} &= -\frac{p_1^2 - p_2^2 + k^2}{2}\\ \frac{dp_2}{ds} &= -p_1 p_2\\ \frac{dk}{ds} &= -p_1 k\end{aligned} \tag{38}$$

They are readily solved

$$\begin{aligned}p_1(s) &= \frac{p_{10} + \frac{s}{2}(k_0^2 + p_{10}^2 + p_{20}^2)}{(1+\frac{s}{2}p_{10})^2 + \frac{s^2}{4}(k_0^2 + p_{20}^2)}\\ p_2(s) &= \frac{p_{20}}{(1+\frac{s}{2}p_{10})^2 + \frac{s^2}{4}(k_0^2 + p_{20}^2)}\\ k(s) &= \frac{k_0}{(1+\frac{s}{2}p_{10})^2 + \frac{s^2}{4}(k_0^2 + p_{20}^2)}\end{aligned} \tag{39}$$

and inverted

$$
\begin{aligned}
p_{10} &= \frac{p_1 - \frac{s}{2}(p_1^2 + p_2^2 + k^2)}{(1 - \frac{s}{2}p_1)^2 + \frac{s^2}{4}(p_2^2 + k^2)} \\
p_{20} &= \frac{p_2}{(1 - \frac{s}{2}p_1)^2 + \frac{s^2}{4}(p_2^2 + k^2)} \\
k_0 &= \frac{k}{(1 - \frac{s}{2}p_1)^2 + \frac{s^2}{4}(p_2^2 + k^2)}
\end{aligned} \tag{40}
$$

We note the identity ($p_0^2 = p_{10}^2 + p_{20}^2$)

$$
\frac{p^2 + k^2}{(1 - \frac{sp_1}{2})^2 + s^2\frac{p_2^2 + k^2}{4}} = p_0^2 + k_0^2 \tag{41}
$$

5.2. Exact determinant

We are now set to evaluate the exact τ-evolution of $\mathbf{\Psi}$. Inserting (38)–(41) into (37) yield

$$
\frac{d\ln\tilde{\mathbf{\Psi}}}{ds} = 2p_1 - \mu^2\left(-\frac{k^2 + p_1^2 - p_2^2}{2} + (p_0^2 + k_0^2)\frac{s^2k^2}{4}\right) \tag{42}
$$

Using (39) into (42) and undoing the derivative, we have

$$
\begin{aligned}
\tilde{\mathbf{\Psi}}(\tau, k, p) = e^{-\mu^2\frac{s\left(-sp_{10}\left(p_0^2+k_0^2\right)-2\left(p_{10}^2-p_{20}^2-k_0^2\right)\right)}{s^2\left(k_0^2+p_0^2\right)+4p_{10}s+4}} \\
\times \frac{\tilde{\mathbf{\Psi}}_0(k_0, p_0)}{\left((1 + \frac{sp_{10}}{2})^2 + s^2\frac{p_{20}^2 + k_0^2}{4}\right)^{-2}}
\end{aligned} \tag{43}
$$

We now re-write (k_0, p_0) in terms of (k, p) and then undo the shifts through $(k \to ik, p \to ip)$. The results are

$$
\begin{aligned}
&\tilde{\mathbf{\Psi}}(\tau, k, p) = \mathbb{K}(\tau, k, p)\tilde{\mathbf{\Psi}}_0(k_0(k, p), p_0(k, p)) \\
&\mathbb{K}(\tau, k, p) = \frac{((2 - p_1s)^2 + s^2(p_2^2 + k^2))^{-2}}{16}e^{-\mu^2\mathbf{S}(k,p,\tau)} \\
&\mathbf{S}(\tau, k, p) = \frac{s\left(sp_1\left(p^2 + k^2\right) - 2\left(p_1^2 - p_2^2 - k^2\right)\right)}{s^2\left(k^2 + p^2\right) - 4p_1s + 4}
\end{aligned} \tag{44}
$$

In terms of the initial variables, the formal solution for $\mathbb{K}$ is

$$
\mathbb{K}(\tau, k_0, p_0) = \frac{e^{-\mu^2\frac{s\left(-sp_{10}\left(p_0^2+k_0^2\right)-2\left(p_{10}^2-p_{20}^2-k_0^2\right)\right)}{s^2\left(k_0^2+p_0^2\right)+4p_{10}s+4}}}{\left((1 + \frac{sp_{10}}{2})^2 + s^2\frac{p_{20}^2 + k_0^2}{4}\right)^{-2}} \tag{45}
$$

The initial condition in Fourier space is

$$
\tilde{\mathbf{\Psi}}_0(k, p) = (\nabla_p^2 + \nabla_k^2)^N\delta^2(k)\delta^2(p) \tag{46}
$$

Thus

$$\mathbf{\Psi}(\tau, z, w) = \left((\nabla_{p_0}^2 + \nabla_{k_0}^2)^N e^{p(p_0,k_0)\cdot z + k(k_0,p_0)\cdot w}\, \mathbb{J}\mathbb{K}(\tau, k_0, p_0)\right)_{p_0=k_0=0} \tag{47}$$

Here, $\mathbb{J} \equiv \mathbb{J}(k, p; k_0, p_0)$ is the Jacobian for the variable transformation $(k_0, p_0) \to (k, p)$ evaluated at (k_0, p_0), i.e.

$$\mathbb{J} \equiv \left(\left(1 + \frac{\tau p_{10}}{2}\right)^2 + \frac{\tau^2}{4}(p_{20}^2 + k_0^2)\right)^{-3} \equiv \frac{1}{F_0^3} \tag{48}$$

Although (47) is exact for finite N, taking the large N limit and assessing its corrections is in general more subtle.

6. Universality at the edge

The depletion of the zeros away from the droplet is captured by the way $\mathbf{\Psi}$ departs from zero away from the sharp boundary. The microscopic and universal changes in the eigenvalue density at the edges are commensurate with the microscopic rate of depletion of the zeros of the characteristic determinant. We now develop a semi-classical expansion in $1/N$ and a pertinent microscopic re-scaling at the edge to show this.

6.1. Saddle point approximation

To explicit this universal behavior, it is more appropriate to insert (44) in (35) and carry a semi-classical expansion around the saddle point in terms of the initial coordinates (k_0, p_0). For notational convenience in this section we will re-label the coordinates (k_0, p_0) by (k, p), and the previous coordinates (k, p) by (K, P). This means that $P \equiv P(p, k)$ and $K \equiv K(p, k)$. With this in mind, we have

$$\mathbf{\Psi}(\tau, z, w) = \int \frac{d^2k}{(2\pi)^2}\frac{d^2p}{(2\pi)^2} d^2z' d^2w' \frac{e^{Nf(\tau,p,k,z,w,z',w')}}{\left((1+\frac{\tau p_1}{2})^2 + \tau^2\frac{p_2^2+k^2}{4}\right)} \tag{49}$$

with

$$f(\tau, p, k, z, w, z', w') = P(p, k)\cdot z + K(p, k)\cdot w - p\cdot z' - k\cdot w' - \mu^2\mathbf{S}(p, k) + \ln(|z'|^2 + |w'|^2) \tag{50}$$

$$\mathbf{S}(p, k) = \frac{p_1 + \frac{\tau}{2}(p_1^2 + p_2^2 - k^2)}{(1+\frac{\tau p_1}{2})^2 + \tau^2\frac{p_2^2+k^2}{4}} - p_1 \tag{51}$$

The saddle point corresponds to $\partial_{z',w',p,k} f = 0$, which are respectively

$$\frac{\partial P}{\partial p} z + \frac{\partial K}{\partial p} w + \mu^2 \frac{\partial S}{\partial p} = z'$$

$$\frac{\partial P}{\partial k} z + \frac{\partial K}{\partial k} w + \mu^2 \frac{\partial S}{\partial k} = w'$$

$$p_i = \frac{2z_i'}{|z'|^2 + |w'|^2}$$
$$k = \frac{2r'}{|z'|^2 + |r'|^2} \tag{52}$$

Near the boundary the first saddle point equation in (52) reduces to

$$(z - \mu^2)\frac{z_0^2}{(\tau + z_0)^2} + \mu^2 = z_0 \tag{53}$$

in agreement with (25). The second saddle point equation in (52) becomes

$$\lim_{r' \to 0}\left(\frac{r'}{k}\right)\frac{2(z_0 + \tau)(\bar{z}_0 + \tau)}{|z_0|^2} =$$
$$\tau\left(4\mu^2 + \frac{z_0 - \mu^2}{z_0}(z_0 + \tau) + \frac{\bar{z}_0 - \mu^2}{z_0}(\bar{z}_0 + \tau)\right) \tag{54}$$

which reduces to (31) after using the last two saddle point equations in (52). In principle, the inversion of the above saddle point equations will determine (z, w) as a function of (z', w'). In practice, this inversion is involved. Fortunately, at the boundary there are simplifications since $(w = 0, w' = 0)$, and since (31) and (52) relate the saddle point initial positions to the current positions.

6.2. Microscopic correction

The correction to the saddle point in momenta will be sought in holomorphic coordinates, i.e

$$p_1 - ip_2 = p$$
$$x_1 p_2 + x_2 p_2 = \frac{1}{2}(pz + \bar{p}\bar{z}) \tag{55}$$

and by expanding around the boundary using the following microscopic rescalings

$$z = z(z_0) + \frac{\delta z}{\sqrt{N}}$$
$$z' = z_0 + \frac{\delta z'}{\sqrt{N}}$$
$$w' = \frac{\delta r'}{N^{\frac{1}{4}}}$$
$$p = p_0(z_0) + \frac{\eta}{\sqrt{N}}$$
$$k = \frac{\omega}{N^{\frac{1}{4}}} \tag{56}$$

The re-scaling in $\delta z'$, $\delta z/\sqrt{N}$ at the boundary is natural, since the droplet area scales as $\mathcal{A} \approx N$ to keep the density of eigenvalues finite, while its length grows as $\sqrt{\mathcal{A}} \approx \sqrt{N}$. Inserting (55)–(56) in (35) and expanding to order N^0 at large N, we obtain

$$N(f - f_0) - \ln\left(\left(1 + \frac{\tau p_1}{2}\right)^2 + \tau^2\frac{p_2^2 + k^2}{4}\right) \approx$$

$$\mathbf{Q}(\eta,\omega,\delta z,\delta z',\delta r') + \sqrt{N}\left(\frac{\delta z}{z_0+\tau}+\frac{\delta\bar z}{\bar z_0+\tau}\right)$$
$$+\sqrt{N}\left(\frac{(\delta r')^2}{|z_0|^2}+\frac{\omega^2|z_0|^2}{4}-\omega\cdot\delta r'\right)$$
$$-\frac{1}{2}\left(\frac{(\delta z')^2}{z_0^2}+\frac{(\delta\bar z')^2}{\bar z_0^2}\right)-(\delta r')^2\left(\frac{\delta z'}{z_0}+\frac{\delta\bar z'}{\bar z_0}\right)-\frac{(\delta r')^4}{2|z_0|^4} \tag{57}$$

with f_0 the value of f in (49) at the saddle point and

$$\mathbf{Q}(\eta,\omega,\delta z,\delta z',\delta r') =$$
$$-\frac{\tau z_0^3(z-\mu^2)}{4(z_0+\tau)^3}\eta^2-\frac{\tau\bar z_0^3(\bar z-\mu^2)}{4(\bar z_0+\tau)^3}\bar\eta^2$$
$$+\left(\frac{z_0^2}{2(z_0+\tau)^2}\delta z-\frac{\delta z'}{2}\right)\eta+\left(\frac{\bar z_0^2}{2(\bar z_0+\tau)^2}\delta\bar z-\frac{\delta\bar z'}{2}\right)\bar\eta$$
$$+\frac{\tau|z_0|^2\omega^2}{4|(z_0+\tau)|^2}\left(\frac{z_0\delta z}{z_0+\tau}+\frac{\bar z_0\delta\bar z}{\bar z_0+\tau}\right)-\frac{\tau^2\omega^4|z_0|^4}{16|(z_0+\tau)|^2}$$
$$-\frac{\tau\omega^2|z_0|^2(\eta(\bar z_0+\tau)(z_0)+\bar\eta(z_0+\tau)\bar z_0}{8|(z_0+\tau)|^2}$$
$$-\frac{\tau^2\omega^2|z_0|^2}{8|z_0+\tau|^2}(\eta(z_0-\mu^2)+\bar\eta(\bar z_0-\mu^2)) \tag{58}$$

Here $z=z(\tau)$ is defined in (25). Under the shift

$$\omega=\frac{2\delta r'}{|z_0|^2}+\alpha \tag{59}$$

the α-integration is subleading and decouples. With this in mind, we can re-structure and simplify $\mathbf{Q}$ in (58) as

$$\mathbf{Q}(\eta,\omega,\delta z,\delta z',\delta r') =$$
$$Q(\eta)+\bar Q(\bar\eta)+(\bar\eta,\eta)\cdot(\bar J,J)+Q_3(\delta r',\delta z)+Q_4(\delta r') \tag{60}$$

with

$$Q(\eta)=-\frac{\tau z_0(z_0-\mu^2)}{4(z_0+\tau)}\eta^2$$
$$J=\frac{1}{2}\frac{z_0^2}{(z_0+\tau)^2}\delta z-\frac{1}{2}\delta z'-\frac{\tau(\delta r')^2((1+\frac{\tau}{\bar z_0})+\tau\frac{z_0-\mu^2}{|z_0|^2})}{2|(z_0+\tau)|^2}$$
$$Q_3=\frac{\tau(\delta r')^2}{|z_0|^2|(z_0+\tau)|^2}\left(\frac{z_0\delta z}{z_0+\tau}+\frac{\bar z_0\delta\bar z}{\bar z_0+\tau}\right)$$
$$Q_4=-\frac{\tau^2(\delta r')^4}{|z_0|^4|z_0+\tau|^2} \tag{61}$$

The partial integration in (49) of the quadratic contribution over (η,ω) gives

$$\mathbf{Q}(\delta z, \delta z', \delta r') =$$
$$+ \frac{J^2}{\frac{\tau z_0(z_0-\mu^2)}{(z_0+\tau)}} + \frac{\bar{J}^2}{\frac{\tau \bar{z}_0(\bar{z}_0-\mu^2)}{(\bar{z}_0+\tau)}} - \frac{\tau^2(\delta r')^4}{|z_0|^4|z_0+\tau|^2}$$
$$+ \frac{\tau(\delta r')^2}{|z_0|^2|(z_0+\tau)|^2}\left(\frac{z_0\delta z}{z_0+\tau} + \frac{\bar{z}_0\delta\bar{z}}{\bar{z}_0+\tau}\right) \tag{62}$$

6.3. Microscopic edge profile

The integration around $\delta z'$ is Gaussian and is readily performed, leaving the last and non-Gaussian integral in $\delta r'$ undone. The result for the characteristic determinant close to the boundary and in the microscopic limit is

$$\Psi(\tau, z(z_0) + \delta z/\sqrt{N}, 0) \approx e^{Nf_0 + \sqrt{N}(\frac{\delta z + \delta\bar{z}}{z_0+\tau})}$$
$$\times \int_0^\infty x dx\, e^{-A(z_0)x^4 + B(z_0,\delta z)x^2 + C(z_0,\delta z)} \tag{63}$$

with

$$A(z_0) = \frac{1}{2|z_0|^4} + \frac{\tau^2}{|z_0|^4|z_0+\tau|^2}$$
$$+ \left(\left(\frac{1}{|z_0|^2 z_0} - \frac{\mathbb{A}}{\mathbb{B}}\right)^2\left(\frac{1}{\mathbb{B}} - \frac{2}{z_0^2}\right)^{-1} - \frac{\mathbb{A}^2}{\mathbb{B}} + \text{c.c.}\right)$$
$$B(z_0, \delta z) = \delta z\left(\frac{\tau z_0}{|z_0|^2|z_0+\tau|^2(z_0+\tau)}\right.$$
$$\left. - 2\mathbb{C}\left(\frac{1}{z_0|z_0|^2} - \frac{2\mathbb{A}}{z_0^2}\right)\left(1 - \frac{2\mathbb{B}}{z_0^2}\right)^{-1}\right) + \text{c.c}$$
$$C(z_0, \delta z) = \frac{z_0^2\delta z^2}{4\tau(z_0-\mu^2)(z_0+\tau)^2}$$
$$\times\left(\frac{z_0}{z_0+\tau} - \frac{1}{\frac{z_0+\tau}{z_0} - \frac{2\tau(z_0-\mu^2)}{z_0^2}}\right) + \text{c.c.} \tag{64}$$

and

$$\mathbb{A} = \frac{\tau((1+\frac{\tau}{\bar{z}_0}) + \tau\frac{z_0-\mu^2}{|z_0|^2})}{2|z_0+\tau|^2}$$
$$\mathbb{B} = \frac{\tau z_0(z_0-\mu^2)}{(z_0+\tau)}$$
$$\mathbb{C} = \frac{z_0^2}{2(z_0+\tau)^2} \tag{65}$$

The depletion of the eigenvalues of the deformed Wishart matrices at the boundary as defined by (25) and (31), follows the product of a Gaussian times an incomplete Error Function (Erfc)

$$\begin{aligned}
&\Psi(\tau, z(z_0) + \delta z/\sqrt{N}, 0) \approx e^{Nf_0 + \sqrt{N}(\frac{\delta z + \delta \bar{z}}{z_0 + \tau})} \\
&\times e^{\frac{B^2(z_0,\delta z)}{4A(z_0,\delta z)} + C(z_0,\delta z)} \int\limits_{\frac{-B(z_0,\delta z)}{2A(z_0)}}^{\infty} dy e^{-A(z_0)y^2} \\
&\equiv e^{Nf_0 + \sqrt{N}(\frac{\delta z + \delta \bar{z}}{z_0 + \tau})} \\
&\times e^{\frac{B^2(z_0,\delta z)}{4A(z_0)} + C(z_0,\delta z)} \operatorname{Erfc}\left(\frac{-B(z_0,\delta z)}{2\sqrt{A(z_0)}}\right)
\end{aligned} \tag{66}$$

Recall that z_0 refers to the boundary value as a solution to (25) and is valid throughout the edge of the deformed Wishart droplet shown in Fig. 2. We note that for $A > 0$

$$\lim_{B \to -\infty} \left(e^{\frac{B^2}{4A}} \operatorname{Erfc}\left(-\frac{B}{2\sqrt{A}}\right)\right) = 0 \tag{67}$$

Eq. (66) is the second main result of this paper.

6.4. Special edge points

The depletion at the edge of the Wishart spectrum (66) translates to a depletion at the edge of the Dirac spectrum. We now make it explicit for the 4 cardinal points where the Dirac droplet crosses the eigenvalue spectrum along the real and imaginary axes, e.g. see Fig. 1. Specifically, the edge of the Dirac droplet on the real axis corresponds to $\mathbf{y}(\tau) = 0$. It maps onto the Wishart boundary point $z_0 = x_0 + i0$ with x_0 in (66) the real solution to

$$x_0^4 - 2\tau\left(\frac{\tau}{2} + \mu^2\right) x_0^2 + 2\mu^2\tau^2 x_0 = 0 \tag{68}$$

In general, the two real solutions to (68) are $x_0 = \tau$ and $x_1/\tau = \frac{1}{2}(-1 - \sqrt{1 + 8\mu^2/\tau})$. They correspond to the outer and inner edge of the Wishart distribution in Fig. 2.

The real solution $x_0 = 1$ yields $x(\tau) = \mu^2 + 4(\tau - \mu^2)$ using (25), which is the outer edge along the real axis in Fig. 2. It maps onto the two outer edges along the real z axis of the Dirac spectrum in Fig. 1 or $\mathbf{z} = \pm 2\sqrt{\tau - \mu^2}$ using the Wishart to Dirac map $z = \mu^2 + \mathbf{z}^2$. The corresponding edge parameters in (64) are

$$\begin{aligned}
A(x_0) &= \frac{(\mu^2 - \tau)^2}{16\mu^2\tau^5} \\
B(x_0) &= \frac{\mu^2 - \tau}{16\mu^2\tau^3}(\delta z + \delta\bar{z}) \\
C(x_0) &= -\frac{1}{32\mu^2\tau}(\delta z^2 + \delta\bar{z}^2)
\end{aligned} \tag{69}$$

and the scaling law (66) on the Wishart envelope is ($\delta z = \delta x + i\delta y$)

$$\begin{aligned}
&\Psi(\tau, z(x_0) + \delta z/\sqrt{N}, 0) \approx \\
&e^{Nf_0}\, e^{\frac{\sqrt{N}\delta x}{\tau}}\, e^{\frac{\delta y^2}{16\mu^2\tau^2}} \operatorname{Erfc}\left(\frac{\delta x}{4\mu\sqrt{\tau}}\right)
\end{aligned} \tag{70}$$

Finally, the real solution $x_1/\tau = \frac{1}{2}(-1 - \sqrt{1 + 8\mu^2/\tau})$ corresponds to the inner edge of the Wishart distribution in Fig. 2 with $z(\tau) < \mu^2$. It maps onto the two outer edges along the imaginary axis of the Dirac spectrum shown in Fig. 1. The corresponding edge parameters in (64) are too lengthy to report here.

6.5. Application to $\mu = \frac{\sqrt{\tau}}{2}$

To be more specific consider the special case of $\mu/\sqrt{\tau} = 1/2$, for which the two real solutions are $z_0 = x_0 = \tau$ and $z_0 = x_0 = -(\sqrt{3}+1)\tau/2$. The first solution corresponds to the outer edge along the real axis of the Wishart spectrum and maps onto the outer edge of the Dirac spectrum also along the real axis. It gives

$$\begin{aligned} A(z_0 = \tau) &= \frac{0.14}{\tau^4} \\ B(z_0 = \tau) &= -\frac{0.19}{\tau^3}(\delta z + \delta \bar{z}) \\ C(z_0 = \tau) &= -\frac{1}{8\tau^2}(\delta z^2 + \delta \bar{z}^2) \end{aligned} \tag{71}$$

The scaling law at the edge of the Wishart spectrum along the real axis is

$$\Psi \approx e^{Nf_0}\, e^{\sqrt{N}\frac{\delta x}{\tau}}\, e^{\frac{\delta y^2}{4\tau^2}}\, \text{Erfc}\left(\frac{0.5\,\delta x}{\tau}\right) \tag{72}$$

The second solution corresponds to the inner edge along the real axis of the Wishart spectrum ($z < \mu^2$) and maps onto the outer edge of the Dirac spectrum along the imaginary axis. It gives

$$\begin{aligned} A(z_0 = -(\sqrt{3}+1)\tau/2) &= \frac{3}{\tau^4} \\ B(z_0 = -(\sqrt{3}+1)\tau/2) &= \frac{11.19}{\tau^3}(\delta z + \delta \bar{z}) \\ C(z_0 = -(\sqrt{3}+1)\tau/2) &= -\frac{6.96}{\tau^2}(\delta z^2 + \delta \bar{z}^2) \end{aligned} \tag{73}$$

with $A > 0$ in this case. Inserting the parameters in (66) we have

$$\Psi \approx e^{Nf_0}\, e^{\sqrt{N}\frac{\delta x}{\tau}}\, e^{27.83\frac{\delta x^2}{\tau^2} + 13.92\frac{\delta y^2}{\tau^2}}\, \text{Erfc}\left(-\frac{6.46\,\delta x}{\tau}\right) \tag{74}$$

6.6. Translation to Dirac

The general result (66) holds around the envelope or boundary of the deformed Wishart ensemble (5) as illustrated in Fig. 2. Its translation to the envelope of the Dirac ensemble as illustrated in Fig. 1, follows from the mapping between the complex eigenvalues or $z = \mu^2 + \mathbf{z}^2$. An infinitesimal displacement δz on the Wishart boundary or $z = z_0 + \delta z/\sqrt{N}$, translates to the infinitesimal displacement $\delta \mathbf{z}$ on the Dirac boundary

$$\begin{aligned} \mathbf{z} &= \mathbf{z}_0 + \frac{\delta \mathbf{z}}{\sqrt{N}} \\ &= \pm\left(z_0 - \mu^2 + \frac{\delta z}{\sqrt{N}}\right)^{\frac{1}{2}} \end{aligned}$$

$$\approx \pm \left(\mathbf{z}_0 + \frac{\delta z}{2(z_0 - \mu^2)^{\frac{1}{2}} \sqrt{N}} \right) \tag{75}$$

Therefore, (66) maps onto the Dirac boundary through the substitution

$$\delta z \to \pm 2 \sqrt{z_0 - \mu^2}\, \delta \mathbf{z} \tag{76}$$

In this spirit, the translation of the Wishart result (70) to Dirac follows using the substitution (76), with $z_0 = \tau$ in this case. The scaling law at the real edge of the Dirac spectrum is sensitive to the chiral condensate, which follows from the large N (mean-field) saddle point of the full or unquenched partition function (1),

$$\begin{aligned} \langle \bar{q} q \rangle &= \lim_{m_f \to 0} \lim_{N \to \infty} \left(-\frac{1}{N N_f} \frac{\partial \ln \mathbf{Z}_{N_F}}{\partial i m_f} \right) \\ &= -2\tau \left(\tau - \mu^2 \right)^{\frac{1}{2}} \end{aligned} \tag{77}$$

which is seen to vanish for $\mu = \mu_c = \sqrt{\tau}$ in the massless case (second order transition). This is remarkable, as it allows for a determination of the physical chiral condensate (77) from the microscopic scaling law at the edge of the quenched Dirac spectrum. Indeed, if we set $\Sigma \equiv |\langle \bar{q} q \rangle|$ at finite μ, the Wishart edge scaling law (70) translates to the Dirac edge scaling law

$$\begin{aligned} &\Psi_D(\tau, \mathbf{z}_0 + \delta \mathbf{z}/\sqrt{N}, 0) \approx \\ &e^{N f_0}\, e^{\sqrt{N} \Sigma \frac{\delta \mathbf{x}}{\tau^2}}\, e^{\Sigma^2 \frac{\delta \mathbf{y}^2}{16 \mu^2 \tau^3}}\, \mathrm{Erfc} \left(\frac{\Sigma}{4 \mu \tau} \frac{\delta \mathbf{x}}{\sqrt{\tau}} \right) \end{aligned} \tag{78}$$

While the exponent in the second factor in (78) grows initially with $\delta \mathbf{x}$, it is countered by the rapid fall off of the complementary error function along the real axis. (78) is vanishingly small for positively large $\delta \mathbf{x}$.

In [24] it was shown that for a class of normal matrices, the spectral density is related to the characteristic determinant for $w \to 0$, with a proportionality factor related to some pertinent weight factor. This result suggests that in our case which is non-normal, the first two factors in (78) may be part of an underlying weight factor as they follow from a standard $1/N$ saddle point approximation, i.e. order N and order N^0. The last factor in (78) does not. It emerges from the specific $1/\sqrt{N}$ level spacing law in (56). We identify it with the edge scaling law for the Dirac spectral density

$$\rho_D(\tau, \mathbf{x}_0 + \delta \mathbf{x}/\sqrt{N}, 0) \approx \frac{1}{2\pi\tau}\, \mathrm{Erfc} \left(\frac{\Sigma}{4 \mu \tau} \frac{\delta \mathbf{x}}{\sqrt{\tau}} \right) \tag{79}$$

In the microscopic limit, the Dirac eigenvalue density along the real-axis follows the universal profile of a complementary error function that is sensitive to the physical chiral condensate Σ at finite μ. Eq. (79) suggests a complementary scaling law for extracting Σ from the Dirac spectrum.

6.7. *Check at the edge point $x_0 = \tau$*

As a way to check on the general result (66) we will re-analyze (49) by trading $(P, K) \leftrightarrow (p, k)$. Using the complex coordinates (55), this amounts to re-writing (49) as

$$\Psi(\tau, z, w) = \int \frac{d^2p d^2k d^2z' d^2w'}{(2\pi)^4} \mathbb{J}\, e^{Nf} \tag{80}$$

with

$$\begin{aligned} f &= \frac{1}{2}pz + \frac{1}{2}\bar{p}\bar{z} + k\cdot r \\ &- P(p,k)z' - \bar{P}(p,k)\bar{z}' - K(p,k)\cdot r' + \frac{\mu^2}{2}(S+\bar{S}) \\ &+ \ln(|z'|^2 + (r')^2) \end{aligned} \tag{81}$$

and

$$\begin{aligned} P(p,k) &= \frac{p(1-\frac{\tau\bar{p}}{2}) - \frac{\tau k^2}{2}}{(1-\frac{\tau p}{2})(1-\frac{\tau\bar{p}}{2}) + \frac{\tau^2k^2}{4}} \\ K(p,k) &= \frac{k}{(1-\frac{\tau p}{2})(1-\frac{\tau\bar{p}}{2}) + \frac{\tau^2k^2}{4}} \\ S(p,k) &= \frac{p(1-\frac{\tau\bar{p}}{2}) + \frac{\tau k^2}{2}}{(1-\frac{\tau p}{2})(1-\frac{\tau\bar{p}}{2}) + \frac{\tau^2k^2}{4}} - p \end{aligned} \tag{82}$$

Here $1/\mathbb{J} = ((1-\frac{\tau p}{2})(1-\frac{\tau\bar{p}}{2}) + \frac{\tau^2k^2}{4})^2$.

Around $x_0 = \tau$ at the boundary, we will use the following microscopic rescaling

$$\begin{aligned} z &= 4\tau - 3\mu^2 + \frac{\eta}{\sqrt{N}},\ p = \tau + \frac{p}{\sqrt{N}},\ k = \frac{k}{N^{1/4}} \\ z' &= \tau + \frac{\delta z'}{\sqrt{N}},\ r' = \frac{r'}{N^{1/4}} \end{aligned} \tag{83}$$

and keep only terms that survive at large N. The result in leading order is

$$N(f - f_0) \approx \frac{\sqrt{N}}{2}(p\eta + \bar{p}\bar{\eta}) + \mathbb{F} \tag{84}$$

with

$$\begin{aligned} \mathbb{F} &= -2p\delta z' - 2\bar{p}\delta z' - \tau(\tau-\mu^2)(p^2+\bar{p}^2) \\ &+ 2\tau k^2(\delta z' + \delta\bar{z}') + 4\tau^3k^2(p+\bar{p}) \\ &+ 2\tau^2k^2(\tau-\mu^2)(p+\bar{p}) - 4\tau^4k^4 - 4\tau k(p+\bar{p})r' \\ &- 4\sqrt{N}kr' + \sqrt{N}(r'/\tau)^2 + 4\sqrt{N}\tau^2k^2 \\ &- \frac{(\delta z')^2 + (\delta\bar{z}')^2}{2\tau^2} - \frac{(r')^4}{2\tau^4} - \frac{(r')^2}{\tau^3}(\delta z' + \delta\bar{z}') \end{aligned} \tag{85}$$

Using the shift $r' = 2k\tau^2 + \frac{\alpha}{N^{1/4}}$, we can convert the r'-integral to an α-integral which is Gaussian and decouples. The $\delta z'$ integral can be undone. The result is

$$\begin{aligned} &\Psi(\tau, 4\tau - 3\mu^2 + \eta/\sqrt{N}, 0) \approx \\ &e^{Nf_0} e^{\sqrt{N}\frac{(\eta+\bar{\eta})}{2\tau}} \int \frac{d^2p d^2k}{(2\pi)^4} e^{\frac{p\eta+\bar{p}\bar{\eta}}{2} + k\cdot r + \mathbb{G}(k,p)} \end{aligned} \tag{86}$$

with

$$\mathbb{G}(k,p) = 2\tau\mu^2(p^2+\bar{p}^2) + 2\tau^2k^2(\tau-\mu^2)(p+\bar{p}) \tag{87}$$

For $r=0$, the momentum integral in (86) gives

$$\int_0^\infty kdk \left| e^{-\frac{1}{8\mu^2}(\frac{\eta}{2}+2\tau^2k^2(\tau-\mu^2))^2} \right|^2$$
$$= \frac{1}{64\pi^2\mu^2(\tau-\mu^2)} e^{\frac{\delta y^2}{16\tau\mu^2}} \operatorname{Erfc}\left(\frac{x}{4\sqrt{\tau}|\mu|}\right) \tag{88}$$

Thus the scaling law for the characteristic determinant at the edge point $x_0=\tau$ and fixed but un-scaled μ, is

$$\Psi(\tau, 4\tau-3\mu^2+\delta z/\sqrt{N}, 0) \approx$$
$$\frac{\tau^2 e^{Nf_0}\, e^{\sqrt{N}\frac{\delta x}{\tau}}}{64\pi^2\mu^2(\tau-\mu^2)}\, e^{\frac{\delta y^2}{16\tau\mu^2}} \operatorname{Erfc}\left(\frac{\delta x}{4\sqrt{\tau}\mu}\right) \tag{89}$$

for the Wishart ensemble and in agreement with (70). The translation to the real edge of the Dirac ensemble follows from the substitution (76). The microscopic scaling law of the characteristic determinant near the real edge of the complex Dirac spectrum (boundary of the zero mode zone) allows for a reading of the quenched chiral condensate (77) by fitting to the universal scaling function (89) or its most general form (115) in Appendix A. This the third main result of this paper.

6.8. *Airy universality at $\mu=0$*

For $\mu\to 0$ the result (89) is singular. This feature is valid throughout the envelope of the Wishart and Dirac spectra. The large N limit and the $\mu=0$ do not commute. Indeed, for $\mu=0$ the spectra are now real, and the new microscopic scaling laws

$$z = 4\tau + \frac{\eta}{N^{\frac{2}{3}}}, \qquad w = \frac{\omega}{N^{\frac{3}{2}}} \tag{90}$$

should replace (83), with the new and re-scaled ansatz

$$\Psi(\tau, 4\tau+\eta/N^{\frac{2}{3}}, \omega/N^{\frac{3}{2}}) \approx$$
$$\tau^{2N} e^{N^{\frac{1}{3}}\frac{(\eta+\bar{\eta})}{2\tau}}\, \psi(\tau,\eta,\bar{\eta},\omega) \tag{91}$$

To order N^2 and $N^{\frac{5}{3}}$, the equation (16) is satisfied identically, irrespective of ψ. At order $N^{\frac{4}{3}}$, the new equation fixes ψ

$$-4\tau(\partial_\eta^2+\partial_{\bar{\eta}}^2)\psi + \frac{1}{4\tau^2}(\eta+\bar{\eta})\psi + 8\tau\partial_{\omega\omega}^2\psi = 0 \tag{92}$$

The general solution to (92) is

$$\int d\lambda\, \kappa(\lambda)\, I_0\left(\sqrt{\frac{\lambda}{8\tau^2}}|\omega|\right) \left|\operatorname{Ai}\left(2^{\frac{2}{3}}\left(\frac{\eta}{4\tau}-\lambda\right)\right)\right|^2 \tag{93}$$

with $\kappa(\lambda)$ a general positive weight. The microscopic determinant at the right edge of the Wishart ensemble involves an Airy kernel. As expected, the mapping through $z=\mathbf{z}^2$ at $\mu=0$ yields an Airy kernel for both edges of the real Dirac spectrum.

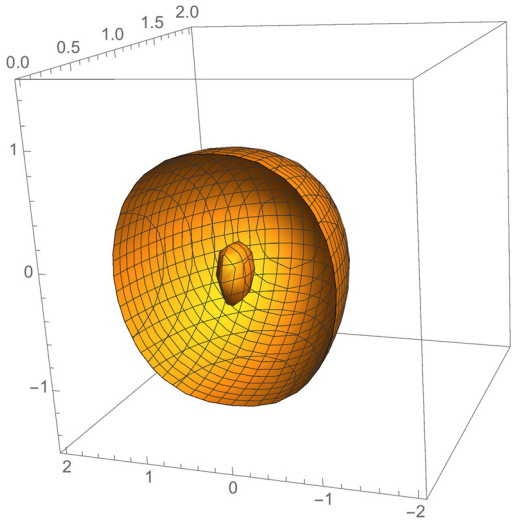

Fig. 3. Saddle point surface $r_0(x_0, y_0)$ viewed along $0 < x_0 < 2$ for $\mu^2 = \frac{1}{4}$ and $\tau = 1$. The lateral axis is y_0, the height is r_0 and the depth is x_0.

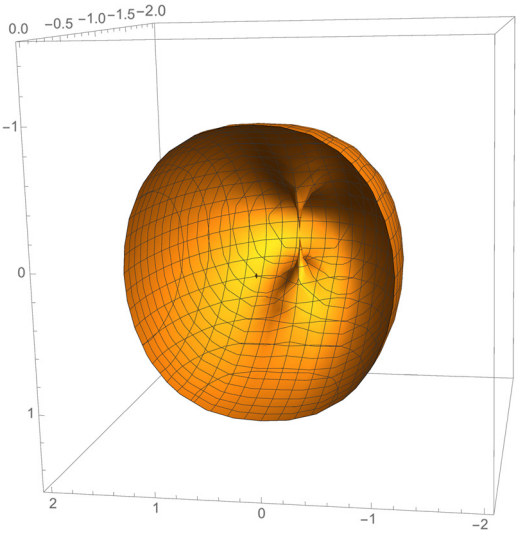

Fig. 4. Saddle point surface $r_0(x_0, y_0)$ viewed along $-2 < x_0 < 0$ for $\mu^2 = \frac{1}{4}$ and $\tau = 1$. The lateral axis is y_0, the height is r_0 and the depth is x_0. The pinch at $r_0(x_0, y_0) \equiv 0(-1, 0)$ is the chiral point in the deformed Wishart spectrum.

7. Chiral universality

The mapping $z = \mathbf{z}^2 + \mu^2$ between the deformed Wishart (z) and Dirac ($\mathbf{z}$) eigenvalues, shows that the zero virtuality point in the Dirac spectrum at finite μ at $\mathbf{z} = 0$, maps onto the $z = \mu^2$ point in the deformed Wishart spectrum. For $\mu/\mu_c < 1$, this point lies within the Dirac and Wishart droplets, and moves out of both droplets for $\mu/\mu_c > 1$. We now analyze the nature of the accumulation of eigenvalues around this point using the characteristic determinant.

7.1. Pinch at zero virtuality

To analyze the saddle point equations (52) in the vicinity of $z \approx \mu^2$ for arbitrary μ^2 and w, we will specialize to the case $\mu^2 = 1/4$ and $\tau = 1$ for simplicity. Throughout this section $\tau = 1$. With this in mind, the second equation in (52) reads

$$\begin{aligned}
&(2x_0 - 2x_0^2 - 10x_0^3 - 2x_0^4 + 8x_0^5 + 4x_0^6 - 6y_0^2 - 10x_0y_0^2 \\
&- 4x_0^2y_0^2 + 16x_0^3y_0^2 + 12x_0^4y_0^2 - 2y_0^4 + 8x_0y_0^4 + 12x_0^2y_0^4 4y_0^6 \\
&- 2r_0^2 - 10x_0r_0^2 - 4x_0^2r_0^2 + 16x_0^3r_0^2 + 12x_0^4r_0^2 \\
&- 4y_0^2r_0^2 + 16x_0y_9^2r_0^2 + 24x_0^2y_0^2r_0^2 + 12y_0^4r_0^2 - 2r_0^4 \\
&+ 8x_0r_0^4 + 12x_0^2r_0^4 + 12y_0^2r_0^4 + 4r_0^6)/D = 0
\end{aligned} \tag{94}$$

with the denominator

$$D \propto x_0(r_0^2 + (x_0+1)^2)(3x_0^2 + x_0^3 + r_0^2 + 3xr^2) \tag{95}$$

The positivity of r_0^2 defines a 3-dimensional surface $r_0(x, 0, y_0)$. In Fig. 4 (front surface) we show a cut of the surface through the plane $x_0 = 0$ for $x_0 < 0$, while in Fig. 3 (back surface) we show a cut of the same surface for $x_0 > 0$. As shown, the front surface is composed of an inner and outer surfaces. In both figures, the side is y_0, the height is r_0 and the depth is x_0. The inner surface excludes a region in parameter space (r_0, x_0, y_0) where no mixed condensate develops. Indeed, for $D \neq 0$ and in the plane $r_0 = 0$ the surface defines a curve

$$\begin{aligned}
&(1 + 2x_0 + x_0^2 + y_0^2) \\
&(x_0 - 3x_0^2 + 2x_0^4 - 3y_0^2 + 4x_0^2y_0^2 + 2y_0^4) = 0
\end{aligned} \tag{96}$$

The second contribution in (96) is the boundary curve (31). It contains two connected pieces also, the inner part is just the intersection between the small island and the (x,y) plane. The first contribution in (96) vanishes at the point $x_0 = -1$, $y_0 = r_0 = 0$ which is where the back surface is pinching the plane $r_0 = 0$ in Fig. 4. This zero is not spurious as can be seen through the plane (x_0, r_0) plane, where (94) simplifies to

$$\begin{aligned}
&(-1 + x_0^2 + r_0^2) \\
&(-x_0 + x_0^2 + 4x_0^3 + 2x_0^4 + r_0^2 + 4x_0r_0^2 + 4x_0^2r_0^2 + 2r_0^4) = 0
\end{aligned} \tag{97}$$

There is a continuous limit to $x_0 = -1$ from the parameter space for a mixed condensate for arbitrary small r_0. The factor $(r_0^2 + x_0^2 - 1)$ cannot be cancelled by the denominator D which is non-vanishing at this point. Thus, the intersection of the condensation region with the real axis shows $x_0 = -1$ as an accumulation point. Now, within the real axis and the branch of the surface determined by $r_0^2 = 1 - x_0^2$, which is the "outer layer" of the condensation region, the first equation for (52) can be solved at once

$$x = \frac{1}{4}(7 + 6x_0) \qquad\qquad y = 0 \tag{98}$$

The point $x_0 = -1$, $y_0 = 0$, $r_0 = 0$ correspond to the chiral point $z = \mu^2 = \frac{1}{4}$. But, at this point, the saddle point momentum and the free energy f in (50) diverge. The chiral point $z = \mu^2$ is a singular point on the surface $r_0 = r_0(x_0, y_0)$ defined by (94), as the outer surface develops two sharp holes that connects through a pinch. The standard $1/N$ expansion breaks down.

7.2. Chiral microscopic universality

To analyze the chiral point more accurately we need an alternative to the standard $1/N$ expansion, that resumes a class of corrections around the chiral point. For that it is useful to go back to (80)–(82) and use the following microscopic rescaling at the chiral point

$$\begin{aligned} &z-\mu^2 \to \frac{z}{N^2}, \mu^2 \to \frac{\mu^2}{N} \\ &w \to \frac{w}{N^2}, p \to Np, k \to Nk \end{aligned} \tag{99}$$

In leading order (80) simplifies

$$\begin{aligned} &\Psi(\tau, \mu^2/N + z/N^2, 0) \approx \\ &\int \frac{d^2pkdkd^2z'd^2w'}{(2\pi)^3} \frac{e^F}{(p^2+k^2)^2} \end{aligned} \tag{100}$$

with

$$\begin{aligned} F \approx &+\frac{N(\bar{z}'+z')}{\tau} + N\ln(|z'|^2+(r')^2) \\ &+\frac{pz+\bar{p}\bar{z}}{2} + kr + 2\frac{\bar{p}z'+p\bar{z}'}{\tau^2(\bar{p}p+k^2)} - \frac{4\mu^2\bar{p}p}{\tau(k^2+\bar{p}p)} \end{aligned} \tag{101}$$

We use the saddle point solution in z', r' to undo this double integration, i.e. $z' = -1+\alpha$ and $r' = 0+\beta$. The resulting Gaussian integrations in α, β decouple. Thus

$$\begin{aligned} &\Psi(\tau, \mu^2/N + z/N^2, 0) \\ &\approx \int \frac{d^2p\,kdk}{(2\pi)^2} \frac{e^{\frac{pz+\bar{p}\bar{z}}{2} - 2\frac{\bar{p}+p}{\tau(\bar{p}p+k^2)} - \frac{4\mu^2\bar{p}p}{(k^2+\bar{p}p)\tau}}}{(p^2+k^2)^2} \end{aligned} \tag{102}$$

The k-integration in (102) can be done by expanding part of the exponent,

$$\begin{aligned} &\Psi(\tau, \mu^2/N + z/N^2, 0) \\ &\approx \int \frac{dpd\bar{p}}{(2\pi)^2} \sum_{n=0}^{\infty} \int kdk \frac{(-2(p+\bar{p}) - 4\mu^2\bar{p}p)^n}{\tau^n(k^2+\bar{p}p)^{n+2}n!} e^{\frac{\bar{p}\bar{z}+pz}{2}} \\ &= \int \frac{dpd\bar{p}}{(2\pi)^2} \sum_{n=0}^{\infty} \frac{1}{\bar{p}p} \frac{(-2(p+\bar{p}) - 4\mu^2\bar{p}p)^n}{\tau^n(n+1)!(\bar{p}p)^n} e^{\frac{\bar{p}\bar{z}+pz}{2}} \\ &= \int_0^1 dt \int \frac{dpd\bar{p}}{(2\pi)^2} \frac{1}{\bar{p}p} e^{-t\frac{2(\bar{p}+p+4\mu^2\bar{p}p)}{\bar{p}p\tau}} e^{\frac{\bar{p}\bar{z}+pz}{2}} \\ &= \int_0^1 dt e^{-\frac{4\mu^2 t}{\tau}} \int \frac{dp}{2\pi p} e^{pz/2 - 2t/p\tau} \int \frac{d\bar{p}}{2\pi\bar{p}} e^{\bar{p}\bar{z}/2 - 2t/\bar{p}\tau} \end{aligned} \tag{103}$$

We note that

$$\xi(z) = \int \frac{dp}{2\pi p} e^{pz/2 - 2t/p\tau} \tag{104}$$

satisfies

$$\left(z\partial_z^2 + \partial_z + \frac{t}{\tau}\right)\xi(z) = 0 \tag{105}$$

$\xi(z) = J_0(2\sqrt{tz/\tau})$ is the unique solution regular at the origin. So as long as we can set the p-integration contour in (103) so that Ψ is regular at $z = 0$, we have $\xi(z) = J_0(2\sqrt{tz/\tau})$. Thus the microscopic form of the characteristic determinant at the chiral point is

$$\begin{aligned}&\Psi(\tau, \mu^2/N + z/N^2, 0) \approx \\ &\approx \tau^{2N} \int_0^1 dt\, e^{-\frac{4\mu^2 t}{\tau}} \left| J_0\left(2\sqrt{\frac{tz}{\tau}}\right)\right|^2\end{aligned} \tag{106}$$

Here μ^2 is short for the fixed combination $N\mu^2$ at large N, as defined through the re-scaling in (99). This is the fourth main result of this paper.

In contrast to (89) the scaling law for the characteristic determinant at the chiral point (106) does not record the quenched chiral condensate at finite μ. We note that (106) is in agreement with the result for the effective partition function in the microscopic limit in [23].

For completeness, we note that (16) simplifies at the chiral point for large N, but fixed $N\mu^2$ and $N^2 z$, i.e. $\mu^2 \to \mu^2/N$, $z \to \mu^2/N + z/N^2$ and $w \to w/N^2$. In the microscopic limit, the resulting differential equation is

$$\begin{aligned}&\Big(2\,(\partial_z + \partial_{\bar z}) + (z\partial_z^2 + \bar z \partial_{\bar z}^2) \\ &- (z + \bar z)\partial_{\bar w w}^2 + (\partial_z + \partial_{\bar z})(w\partial_w + \bar w \partial_{\bar w}) \\ &+ \frac{4\mu^2}{\tau}\frac{(\partial_z + \partial_{\bar z})\,\partial_{\bar w w}^2}{(\partial_z\partial_{\bar z} + \partial_{\bar w w}^2)}\Big)\mathbf{\Psi} \approx \mathbf{0}\end{aligned} \tag{107}$$

The solution to (107) as $w \to 0$ is (106).

8. Conclusions

The QCD Dirac spectrum at finite chemical potential contains subtle information on the chiral dynamics of light quarks in matter. Using a random matrix model, we have shown that the characteristic determinant of phase quenched QCD with $N_f = 2$ massless quarks is related to the characteristic determinant of a class of deformed Wishart matrices through a conformal mapping in the space of eigenvalues.

We have constructed a stochastic evolution for the deformed Wishart matrices by allowing the Gaussian weights in random matrices to diffuse. The mathematical diffusion time is identified with the stochastic time. We have derived an exact solution to the stochastic diffusion equation for any finite N and derived the explicit time-evolving boundary condition of the envelope of the deformed Wishart eigenvalues through a semi-classical expansion.

Contrary to the lore of random matrix approaches to QCD [25], which focus on the spectral density distributions of the Dirac operator, we studied here the characteristic determinant. Following a recent observation in [15], that the spectral evolution of non-Hermitean and non-normal ensembles involves a hidden complex variable w [13], we have embedded the Dirac operator into

this general algebraic structure. The explicit dependence on w is key to closing and obtaining the main evolution equations (16)–(120). While the complex variable z reflects on the standard quark condensate, the complex variable w reflects on the "spurious" quark condensate [9,10,13], whose formation is an artifact of quenching or ignoring the phase of the fermionic determinant. This evolution equation is exact for any finite N. This fact allows to trace the co-evolution of both type of condensates, and to perform all kinds of rescalings in the vicinity of the physically pertinent points.

In general, the complex eigenvalues form a droplet in the complex eigenvalue plane that breaks conformal symmetry. The deformed Wishart droplet deforms but never breaks. Its boundary is sharp at large N, and smoothens out in $1/N$ through a universal edge function in leading order. At the chiral point, the characteristic determinant follows universally from a pertinent Bessel kernel.

The edge universality and the chiral universality derived in this work can be numerically checked. In particular, the microscopic scaling law at the edge of the spectrum scales with the chiral condensate at finite μ, allowing for its possible extraction directly from current and quenched lattice data. In practice and in the absence of an apparent edge in real QCD spectra, this can be achieved by rescaling the numerical eigenvalues within a sliding window along the real axis, and checking for the edge scaling law for the Dirac spectrum using for instance (78)–(79), or along the w-axis using (115)–(116). When extended to finite temperature and finite current quark masses, this practical analysis will allow for a determination of the QCD phase diagram solely from the quenched lattice simulations, without having to solve the QCD sign problem, a major achievement in this field.

Finally and on general grounds, most of our results for the deformed Wishart ensemble may be of relevance to a wider audience of practitioners using non-hermitean random matrix methods in the fields of wireless communication, biological and neural information, and finance [18].

Acknowledgements

We thank Piotr Warchoł and Jacek Grela for a discussion. We would like to thank the organizers of the Workshop on Random Matrix Theory, Integrable Systems, and Topology in Physics organized at the Simons Center for Geometry and Physics at Stony Brook, where this work was initiated. This work is supported in part by the U.S. Department of Energy under Contracts No. DE-FG-88ER40388 (YL and IZ) and by the Grant DEC-2011/02/A/ST1/00119 of the National Center of Science and by the grant from the Simons Foundation (MAN).

Appendix A

It is instructive to re-check the edge scaling laws (63)–(66) near $x_0/\tau = 1$ directly from (16). Recall that this point maps onto the outer edge $z(\tau) = 4\tau - 3\mu^2$ in the Wishart ensemble and $\mathbf{z}(\tau) = \pm 2\sqrt{\tau - \mu^2}$ in the Dirac ensemble. At $x_0 = \tau$, the leading contribution to the characteristic determinant in large N is

$$f_0 = \frac{-2\mu^2}{\tau} + 2\ln\tau \tag{108}$$

Inserting the re-scaling

$$z(\tau) = 4\tau - 3\mu^2 + \frac{\eta}{N^{\frac{1}{2}}}, \qquad w = \frac{\omega}{N^{\frac{3}{4}}} \tag{109}$$

and the re-scaled ansatz

$$\Psi(\tau, 4\tau - 3\mu^2 + \eta/N^{\frac{1}{2}}, \omega/N^{\frac{3}{4}}) \approx \tau^{2N} e^{-\frac{2N\mu^2}{\tau}} e^{\frac{\sqrt{N}}{2\tau}(\eta+\bar{\eta})} \varphi(\tau, \eta, \bar{\eta}, \omega) \tag{110}$$

in (63)–(66), yield the identity to order N^2

$$\left(\frac{2\mu^2}{\tau^2} - \frac{2}{\tau}\right)\varphi = \left(\frac{2\mu^2}{\tau^2} - \frac{2}{\tau}\right)\varphi \tag{111}$$

which is satisfied whatever φ. At order $N^{\frac{3}{2}}$, φ is fixed by

$$(8\tau - 8\mu^2)\partial^2_{\omega\omega}\varphi + \frac{4\mu^2}{\tau}(\partial_\eta + \partial_{\bar{\eta}})\varphi + \frac{1}{4\tau^2}(\bar{\eta} + \eta)\varphi = 0 \tag{112}$$

The formal solution to (112) is

$$\varphi(\tau, \eta, \bar{\eta}, \omega) \approx \int_0^\infty d\lambda\, \kappa(\lambda)\, I_0\left(\frac{\sqrt{\lambda}|\omega|}{\sqrt{2(\tau - \mu^2)}}\right) e^{-\frac{\tau}{4\mu^2}(\frac{\eta+\bar{\eta}}{4\tau} + \lambda)^2} g(\tau, \eta - \bar{\eta}) \tag{113}$$

with arbitrary positive weight κ and arbitrary g. A comparison of (113) to (88) fixes κ and g to be respectively

$$\kappa(\lambda) \approx \frac{\tau}{(\tau - \mu^2)}$$
$$g(\tau, \eta - \bar{\eta}) \approx e^{-\frac{(\eta-\bar{\eta})^2}{64\tau\mu^2}} \tag{114}$$

Thus

$$\Psi(\tau, 4\tau - 3\mu^2 + \eta/N^{\frac{1}{2}}, \omega/N^{\frac{3}{4}}) \approx \tau^{2N+1} \frac{e^{-\frac{2N\mu^2}{\tau}} e^{\frac{\sqrt{N}}{2\tau}(\eta+\bar{\eta})}}{(\tau - \mu^2)} \times \int_0^\infty d\lambda\, I_0\left(\frac{\sqrt{\lambda}|\omega|}{\sqrt{2(\tau - \mu^2)}}\right) e^{-\frac{\tau}{4\mu^2}(\frac{\eta+\bar{\eta}}{4\tau} + \lambda)^2 - \frac{(\eta-\bar{\eta})^2}{64\tau\mu^2}} \tag{115}$$

Eq. (115) shows that along the ω-direction, the characteristic determinant at the real edge of the Wishart and therefore the Dirac spectrum through (76) for $x_0 = \tau$, scales with the chiral condensate (77). Thus the edge scaling law (115) allows for a possible measurement of the chiral condensate at the edge of the complex eigenvalue droplet along the w-direction,

$$\Psi_D(\tau, \mathbf{z}_0, \omega/N^{\frac{3}{4}}) \approx \tau^{2N+1} \frac{e^{-\frac{2N\mu^2}{\tau}}}{(\tau - \mu^2)} \int_0^\infty d\lambda\, I_0\left(\frac{\sqrt{\lambda}|\omega|}{\sqrt{2(\tau - \mu^2)}}\right) e^{-\frac{\tau\lambda^2}{4\mu^2}} \tag{116}$$

Eq. (116) is the analogue of (78) along the w-direction.

Appendix B

In this Appendix we will show that the characteristic determinant for the 2-matrix model [11,12] obeys a closed form equation analogous to (16) and share the same microscopic universality near the chiral Dirac point. For that, we define

$$\mathbf{\Phi}(\tau, z, w) = \left\langle \det\left((z - \mathbb{W})(\bar{z} - \bar{\mathbb{W}}) + |w|^2\right)\right\rangle \tag{117}$$

with the newly deformed and non-hermitean Wishart-like matrix

$$\mathbb{W} = (\mathbf{A}^\dagger - i\mu\mathbf{B}^\dagger)(\mathbf{A} - i\mu\mathbf{B}) \tag{118}$$

The relationship between the 2-matrix Dirac spectrum at finite μ with eigenvalues $\mathbf{z}$ and the newly deformed Wishart $\mathbb{W}$ spectrum with eigenvalues z is through the new mapping $z = \mathbf{z}^2$. The averaging in (117) is now carried using the double Gaussian weight

$$\mathbf{P}(\tau, \mathbf{A}, \mathbf{B}) \approx e^{-\frac{N}{\tau}\mathrm{Tr}(\mathbf{A}^\dagger\mathbf{A} + \mathbf{B}^\dagger\mathbf{B})} \tag{119}$$

Using the same arguments as those developed above, we unwind $\partial_\tau \mathbf{\Phi}$ in terms of Grassmannians, undo the $\mathbf{A}, \mathbf{B}$ integrations and carry the Grassmannian integrations by trading them with partial derivatives in $(z, \bar{z}, w, \bar{w})$. The result is a closed form equation

$$\begin{aligned}
&N\partial_\tau \mathbf{\Phi} = -2(\partial_z + \partial_{\bar{z}})\mathbf{\Phi} \\
&+ \left(\frac{\mu^2}{\tau} - 1\right) \\
&\times \left(z\partial_z^2 + \bar{z}\partial_{\bar{z}}^2 + \frac{1}{2}(\partial_z + \partial_{\bar{z}})(w\partial_w + \bar{w}\partial_{\bar{w}})\right)\mathbf{\Phi} \\
&+ \left(\left(1 + \frac{\mu^2}{\tau}\right)\right. \\
&\times \left.\left((z + \bar{z})\partial_{\bar{w}w}^2 - \frac{1}{2}(\partial_z + \partial_{\bar{z}})(w\partial_w + \bar{w}\partial_{\bar{w}})\right)\right)\mathbf{\Phi} \\
&+ \left(\left(1 - \frac{\tau}{N}(\partial_z + \partial_{\bar{z}})\right) + \frac{4\mu^2}{\tau}\left(1 + \frac{\mu^2}{\tau}\right)\partial_{\bar{w}w}^2\right) \\
&\times \left(\left|1 + \left(\frac{\mu^2}{\tau} - 1\right)\frac{\tau}{N}\partial_z\right|^2 + \left|\left(1 + \frac{\mu^2}{\tau}\right)\frac{\tau}{N}\partial_w\right|^2\right)^{-1}\mathbf{\Phi}
\end{aligned} \tag{120}$$

which is the analogue of (16) for the 2-matrix model. Here, the chiral point in the Dirac spectrum or $\mathbf{z} = 0$ maps onto the Wishart point $z = 0$. Using a similar microscopic re-scaling or $z \to \frac{z}{N^2}$, $w \to \frac{w}{N^2}$ around the chiral point in (120) yields (107). The characteristic determinant for both the 1-matrix and 2-matrix models shares the same microscopic universality at the chiral point. This observation extends to the characteristic determinant the universality noted at the chiral point for the microscopic density for both the 1- and 2-matrix models [23].

References

[1] M.A. Nowak, M. Rho, I. Zahed, Chiral Nuclear Dynamics, World Scientific, Singapore, 1996, 528 pp.
[2] C. Bernard, C.E. DeTar, L. Levkova, S. Gottlieb, U.M. Heller, J.E. Hetrick, J. Osborn, D.B. Renner, et al., PoS LAT 2007 (2007) 090, arXiv:0710.1118 [hep-lat].

[3] T. Banks, A. Casher, Nucl. Phys. B 169 (1980) 103.
[4] R.A. Janik, M.A. Nowak, G. Papp, I. Zahed, Phys. Rev. Lett. 81 (1998) 264, arXiv:hep-ph/9803289;
R.A. Janik, M.A. Nowak, G. Papp, I. Zahed, Prog. Theor. Phys. Suppl. 131 (1998) 471;
R.A. Janik, M.A. Nowak, G. Papp, I. Zahed, in: J. Tran Thanh Van (Ed.), The Proceedings, 34th Rencontres de Moriond, The Gioi, Hanoi, 2001, arXiv:hep-ph/9905274.
[5] E.V. Shuryak, J.J.M. Verbaarschot, Nucl. Phys. A 560 (1993) 306, arXiv:hep-th/9212088;
J.J.M. Verbaarschot, I. Zahed, Phys. Rev. Lett. 70 (1993) 3852, arXiv:hep-th/9303012.
[6] M.A. Nowak, J.J.M. Verbaarschot, I. Zahed, Phys. Lett. B 217 (1989) 157.
[7] H. Leutwyler, Phys. Lett. B 189 (1987) 197;
R.A. Janik, M.A. Nowak, G. Papp, I. Zahed, Acta Phys. Pol. B 29 (1998) 3957, arXiv:hep-ph/9812376;
L. Giusti, M. Luscher, P. Weisz, H. Wittig, J. High Energy Phys. 0311 (2003) 023, arXiv:hep-lat/0309189;
H. Fukaya, et al., TWQCD Collaboration, Phys. Rev. D 76 (2007) 054503, arXiv:0705.3322 [hep-lat];
F. Basile, G. Akemann, J. High Energy Phys. 0712 (2007) 043, arXiv:0710.0376 [hep-th].
[8] A. Gocksch, Phys. Rev. Lett. 61 (1988) 2054;
I. Barbour, N.E. Behilil, E. Dagotto, F. Karsch, A. Moreo, M. Stone, H.W. Wyld, Nucl. Phys. B 275 (1986) 296;
I.M. Barbour, S.E. Morrison, E.G. Klepfish, J.B. Kogut, M.P. Lombardo, Nucl. Phys. Proc. Suppl. 60A (1998) 220, arXiv:hep-lat/9705042.
[9] M.A. Stephanov, Phys. Rev. Lett. 76 (1996) 4472, arXiv:hep-lat/9604003.
[10] R.A. Janik, M.A. Nowak, G. Papp, I. Zahed, Phys. Rev. Lett. 77 (1996) 4876, arXiv:hep-ph/9606329.
[11] J.C. Osborn, Phys. Rev. Lett. 93 (2004) 222001, arXiv:hep-th/0403131.
[12] G. Akemann, J. Phys. A 36 (2003) 3363, arXiv:hep-th/0204246;
G. Akemann, Acta Phys. Pol. B 38 (2007) 3981, arXiv:0710.2905 [hep-th].
[13] R.A. Janik, M.A. Nowak, G. Papp, I. Zahed, Phys. Lett. B 440 (1998) 123, arXiv:hep-ph/9806479;
R.A. Janik, M.A. Nowak, G. Papp, I. Zahed, in: New Developments in Quantum Field Theory, Zakopane, 1997, pp. 297–314, arXiv:hep-ph/9708418;
R.A. Janik, M.A. Nowak, G. Papp, I. Zahed, Acta Phys. Pol. B 28 (1997) 2949, arXiv:hep-th/9710103;
R.A. Janik, M.A. Nowak, G. Papp, J. Wambach, I. Zahed, Phys. Rev. E 55 (1997) 4100, arXiv:hep-ph/9609491;
R.A. Janik, M.A. Nowak, G. Papp, I. Zahed, Nucl. Phys. B 501 (1997) 603, arXiv:cond-mat/9612240.
[14] A.M. Halasz, J.C. Osborn, J.J.M. Verbaarschot, Phys. Rev. D 56 (1997) 7059, arXiv:hep-lat/9704007;
J.J.M. Verbaarschot, Nucl. Phys. A 642 (1998) 305, arXiv:hep-ph/9807296;
F. Basile, G. Akemann, J. High Energy Phys. 0712 (2007) 043, arXiv:0710.0376 [hep-th];
K. Splittorff, J.J.M. Verbaarschot, Phys. Rev. D 75 (2007) 116003, arXiv:hep-lat/0702011 [hep-lat];
J. Han, M.A. Stephanov, Phys. Rev. D 78 (2008) 054507, arXiv:0805.1939 [hep-lat];
H. Fujii, T. Sano, Phys. Rev. D 83 (2011) 014005, arXiv:1009.5977 [hep-ph];
G. Akemann, T. Kanazawa, M.J. Phillips, T. Wettig, J. High Energy Phys. 1103 (2011) 066, arXiv:1012.4461 [hep-lat];
A. Mollgaard, K. Splittorff, Phys. Rev. D 91 (3) (2015) 036007, arXiv:1412.2729 [hep-lat].
[15] J.P. Blaizot, M.A. Nowak, P. Warchoł, Phys. Rev. E 89 (4) (2014) 042130;
J.P. Blaizot, M.A. Nowak, P. Warchoł, Phys. Lett. B 724 (2013) 170, arXiv:1303.2357 [hep-ph];
J.P. Blaizot, M.A. Nowak, P. Warchoł, Phys. Rev. E 89 (4) (2014) 042130;
Z. Burda, J. Grela, M.A. Nowak, W. Tarnowski, P. Warchoł, Phys. Rev. Lett. 113 (2014) 104102;
Z. Burda, J. Grela, M.A. Nowak, W. Tarnowski, P. Warchoł, Nucl. Phys. B 897 (2015) 421;
J.P. Blaizot, J. Grela, M.A. Nowak, P. Warchoł, Acta Phys. Pol. B 46 (9) (2015) 1785;
J. Grela, J. Phys. A, Math. Theor. 49 (2015) 015201;
J.P. Blaizot, J. Grela, M.A. Nowak, W. Tarnowski, P. Warchoł, arXiv:1512.06599 [math-ph].
[16] Y. Liu, P. Warchoł, I. Zahed, arXiv:1505.02107 [hep-ph], 2015;
Y. Liu, P. Warchoł, I. Zahed, arXiv:1506.08787 [hep-ph], 2015;
P.J. Forrester, J. Grela, J. Phys. A, Math. Theor. 49 (2016) 085203, arXiv:1507.07274 [math-ph].
[17] J. Gasser, H. Leutwyler, Phys. Lett. B 188 (1987) 477;
J. Gasser, H. Leutwyler, Phys. Lett. B 184 (1987) 83.
[18] K. Rajan, L.F. Abbot, Phys. Rev. Lett. 97 (2006) 188104;
Ch. Biely, S. Thurner, Quant. Finance 8 (2008) 705;
F. Krzakala, et al., Proc. Natl. Acad. Sci. USA 110 (2013) 20935;
R. Couillet, M. Debbah, Random Matrix Methods for Wireless Communications, Cambridge University Press, 2011;
H. Rouault, S. Druckmann, arXiv:1509.01983 [q-bio.NC], 2015.

[19] I. Barbour, N.E. Behilil, E. Dagotto, F. Karsch, A. Moreo, M. Stone, H.W. Wyld, Nucl. Phys. B 275 (1986) 296.
[20] H. Markum, R. Pullirsch, T. Wettig, Phys. Rev. Lett. 83 (1999) 484, arXiv:hep-lat/9906020.
[21] Y. Liu, I. Zahed, arXiv:1509.00812 [hep-ph], 2015.
[22] J.C. Osborn, K. Splittorff, J.J.M. Verbaarschot, Phys. Rev. Lett. 94 (2005) 202001, arXiv:hep-th/0501210.
[23] K. Splittorff, J.J.M. Verbaarschot, Nucl. Phys. B 683 (2004) 467;
J.J.M. Verbaarschot, in: E. Brezin, et al. (Eds.), The Proceedings, NATO Advanced Study Institute, Les Houches, Springer, Dordrecht, 2006, arXiv:hep-th/0502029.
[24] G. Akemann, G. Vernizzi, Nucl. Phys. B 660 (2003) 532, arXiv:hep-th/0212051.
[25] For a review, see: J.J.M. Verbaarschot, in: G. Akemann, J. Baik, Ph. Di Francesco (Eds.), Oxford Handbook of Random Matrix Theory, OUP, Oxford, 2015.